THE ORIGIN AND SIGNIFICANCE OF REVERSE ZONING IN MELILITE FROM ALLENDE TYPE B INCLUSIONS[1]

GLENN J. MACPHERSON[2], JULIE M. PAQUE, EDWARD STOLPER, AND LAWRENCE GROSSMAN[3]
Department of the Geophysical Sciences, University of Chicago, 5734 South Ellis Avenue, Chicago, IL 60637
Division of Geological and Planetary Sciences, California Institute of Technology, Pasadena, CA 91125
Division of Geological and Planetary Sciences, California Institute of Technology, Pasadena, CA 91125
Department of the Geophysical Sciences, University of Chicago, 5734 South Ellis Avenue, Chicago, IL 60637

ABSTRACT

In many Type B Allende inclusions, melilite is reversely-zoned over restricted portions of each crystal. Textural relationships and the results of dynamic crystallization experiments suggest that the reversely-zoned intervals in these Type B melilites result from the co-precipitation of melilite with clinopyroxene from a melt, prior to the onset of anorthite precipitation. When clinopyroxene begins to precipitate, the Al/Mg ratio of the melt rises, causing the crystallizing melilite to become more gehlenitic, an effect which is negated by crystallization of anorthite. Because the equilibrium crystallization sequence in these liquids is anorthite before pyroxene, melilite reverse zoning can occur only when anorthite nucleation is suppressed relative to pyroxene. This has been achieved in our experiments at cooling rates as low as 0.5°C/hour. Our experiments further indicate, however, that reverse zoning does not form at cooling rates $\geq$50°C/hour, probably because the clinopyroxene becomes too Al-rich to drive up the Al/Mg ratio of the liquid. Type B inclusions with reversely-zoned melilites must have cooled at rates greater than those at which anorthite begins to crystallize before clinopyroxene but <50°C/hour. Such rates are far too slow for the Type B droplets to have cooled by radiation into a nebular gas but are much faster than the cooling rate of the solar nebula itself. One possibility is that Type B's formed in local hot regions within the nebula, where their cooling rate was equal to that of their surrounding gas. Other possibilities are that their cooling rates reflect their movement along nebular temperature gradients or the influence of a heat source. The sun or viscous drag on inclusions as they moved through the nebular gas are potential candidates for such heat sources.

INTRODUCTION

Coarse-grained Ca-, Al-rich inclusions in Allende and other carbonaceous chondrite meteorites are thought to have formed in the primordial solar nebular cloud prior to the formation of planets. Grossman (1975) classified these inclusions into two kinds, Type A and Type B. The primary phases in Type A inclusions are Na-, Fe-free melilite; Mg-, Al-spinel and minor hibonite ($CaAl_{12}O_{19}$) and perovskite. Type B inclusions consist mostly of Fe-free, Ti-, Al-rich clinopyroxene (fassaite); Mg-, Al-spinel; melilite; and anorthite. Wark and Lovering (1977) further subdivided the Type B's into B1's, which have melilite mantles, and B2's, which do not. For detailed petrographic descriptions of coarse-grained Ca-, Al-rich inclusions and for a review of their significance in deciphering the early history of the solar system, see Grossman (1975) and Grossman (1980), respectively.

Zoned melilite crystals with compositions that can be almost perfectly represented by the binary system åkermanite ($Ca_2MgSi_2O_7$)—gehlenite ($Ca_2Al_2SiO_7$) are major constituents of most of these inclusions. Detailed interpretation of the zoning patterns in, and textural relationships of, the melilites in these objects has played an important part in efforts to understand their origin and evolution. For example, melilite crystals that radiate inward from the rims of Type B1 inclusions and that are zoned from gehlenite- to åkermanite-rich compositions along their lengths from the rims of the inclusions toward their interiors have been interpreted as indicating that these objects crystallized from melt droplets (MacPherson and Grossman 1981). This zoning pattern in gehlenitic melilites is usually referred to as "normal" since it is the zoning pattern expected in melilites crystallized

[1] Manuscript received October 7, 1983; revised January 31, 1984.

[2] Present address: Dept. of Mineral Sciences, Smithsonian Institution, Washington, D.C.

[3] Also: Enrico Fermi Inst., University of Chicago.

[JOURNAL OF GEOLOGY, 1984, vol. 92, p. 289–305]

0022-1376/84/9203-006$1.00

from gehlenitic liquids with falling temperature according to the binary phase diagram of Osborn and Schairer (1941). In contrast, many Type A inclusions have melilites that are "reversely-zoned"; i.e., that are very gehlenitic overall but which become progressively less åkermanite-rich from their cores to their rims. This feature, difficult to reconcile with crystallization from a melt, has been attributed to condensation from a gas as the pressure in the nebula decreased (Allen and Grossman 1978; MacPherson and Grossman 1983). Metamorphism in planetary environments has also been invoked to explain some of the complex textural and zoning patterns involving melilites in coarse-grained inclusions in Allende (Meeker et al. 1983*b*).

In this paper, we describe what may at first appear to be a curious but insignificant feature of many of the melilites of Type B inclusions. Although most reports in the literature suggest that melilites in these inclusions show normal zoning patterns, we have found that many of the melilites show reverse zoning over restricted portions of each crystal, in contrast to those in Type A's, which are reversely-zoned throughout. We also report the results of dynamic crystallization experiments on compositions similar to an average Type B inclusion in which reversely-zoned melilite rims were grown on normally-zoned cores, like the zoning in many natural Type B melilites. We interpret the fact that we have been able to duplicate these reverse zoning patterns as evidence that natural melilites having such zoning were formed by crystallization from a melt. Furthermore, reverse zoning could only be produced in our experiments over a restricted range of experimental conditions. Thus, the presence in natural inclusions of the kinds of zoning patterns described herein may place valuable constraints on the conditions under which the inclusions formed.

ANALYTICAL TECHNIQUES

All samples described herein were examined optically and analyzed with an ARL-EMX-SM automated, three-spectrometer electron microprobe, equipped with a Nuclear Semiconductor AUTOTRACE Si (Li) X-ray detector. Analytical procedures were similar to those described in Allen et al. (1978). Step-scans were done using energy-dispersive analysis, 60-second counting times, and 10–20 μm intervals. Melilite compositions were calculated using Al and Si data only, because the poor counting statistics for Mg generally gave discrepant values. Reproducibility of analyses and comparison with wavelength-dispersive analyses performed on the same melilite crystals indicate that melilite compositions obtained by our technique are accurate to better than ±3 mole % gehlenite.

The experimental techniques and results of our dynamic crystallization experiments are summarized in Paque and Stolper (1983) and will be described in detail in a future publication.

DESCRIPTIONS OF TYPE B INCLUSIONS

Descriptions of melilite in Allende Type B inclusions (e.g., Blander and Fuchs 1975; Wark and Lovering 1982) frequently note the wide range of composition within a particular inclusion, but zoning patterns within single crystals are seldom described in detail. In the few cases that have been described, the zoning pattern is generally one of a gehlenite-rich core grading outward to an åkermanite-rich rim (Grossman 1975; MacPherson and Grossman 1981), i.e., normal zoning. Careful reexamination of melilite in many Type B's has shown that, while the melilite crystals in a few inclusions such as the one described by MacPherson and Grossman (1981) are indeed normally-zoned, melilite in many others shows reverse zoning. This zoning pattern was recognized in previous work (e.g., El Goresy et al. 1979; Meeker et al. 1983*b*), but no detailed description or discussion of its possible origin and significance has been presented.

Figure 1 shows an example of such a melilite crystal from a Type B1 inclusion, designated TS23F1, and the composition profile measured during an electron microprobe traverse across the crystal. This large (~1.5 mm in length) melilite crystal has the composition Geh ~ 73 at its core, and the gehlenite content decreases smoothly outward over most of the distance to the rim, reaching Geh ~ 28. Abruptly at that point, however, the gehlenite content begins to *increase* outwards, reaches a maximum of Geh ~ 48, drops to Geh ~ 40 and rises again to Geh ~ 46 before sharply declining once more at the outermost rim (Geh ~ 32). As shown in figure 1, this zoning pattern can be seen easily with

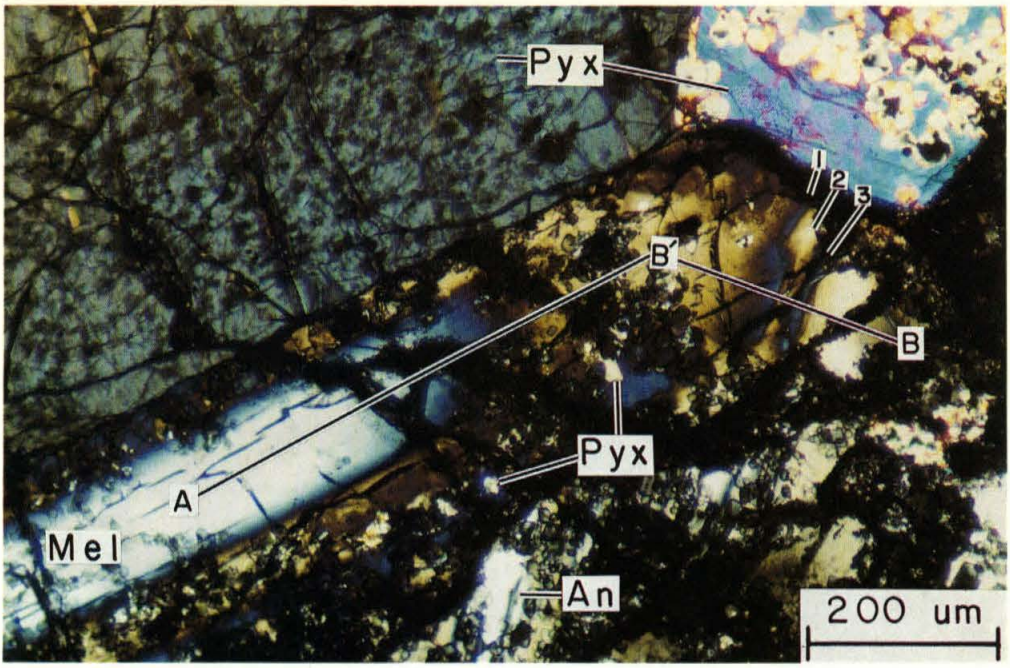

FIG. 1*a*.—Photomicrograph of a large melilite (Mel) crystal in the Type B1 inclusion TS23F1. In this photo and in figs. 2*a*–4*a*, the lines marked *A*–*B* are the locations on the electron microprobe step-scan profiles. The melilite crystal is normally-zoned outwards from its core (*A*; blue-white interference color) to *B'* (olive brown), reversely-zoned from *B'* to the center of the anomalous blue band marked *1*, normally-zoned from *1* to the center of the olive brown band marked *2*, reversely-zoned from *2* to the center of the band marked *3*, and normally-zoned from *3* out to the rim (*B*). Note that pyroxene (Pyx) inclusions are abundant in the outer parts of the melilite but absent from its core. This and succeeding photomicrographs taken with crossed polarizers. Other abbreviations: An—anorthite.

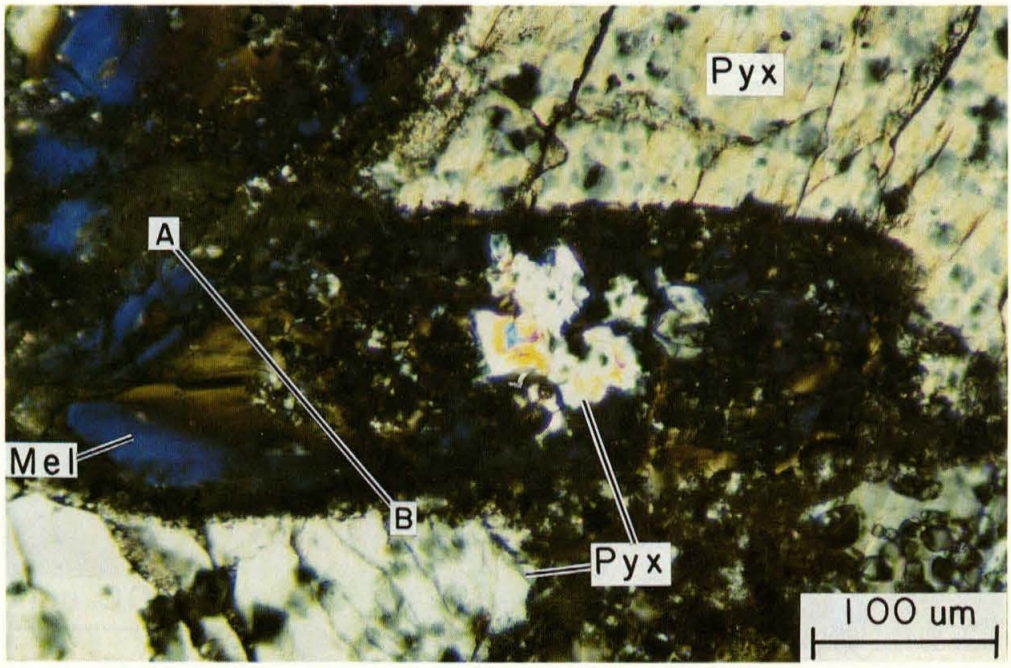

FIG. 2*a*.—Photomicrograph of a small melilite crystal, also in TS23F1. The melilite is reversely-zoned from its core (olive-brown) outwards, with only the outermost rim showing normal zoning. Large pyroxene inclusions are present in the core of this melilite, in contrast to the crystal in figure 1. Abbrev. as before.

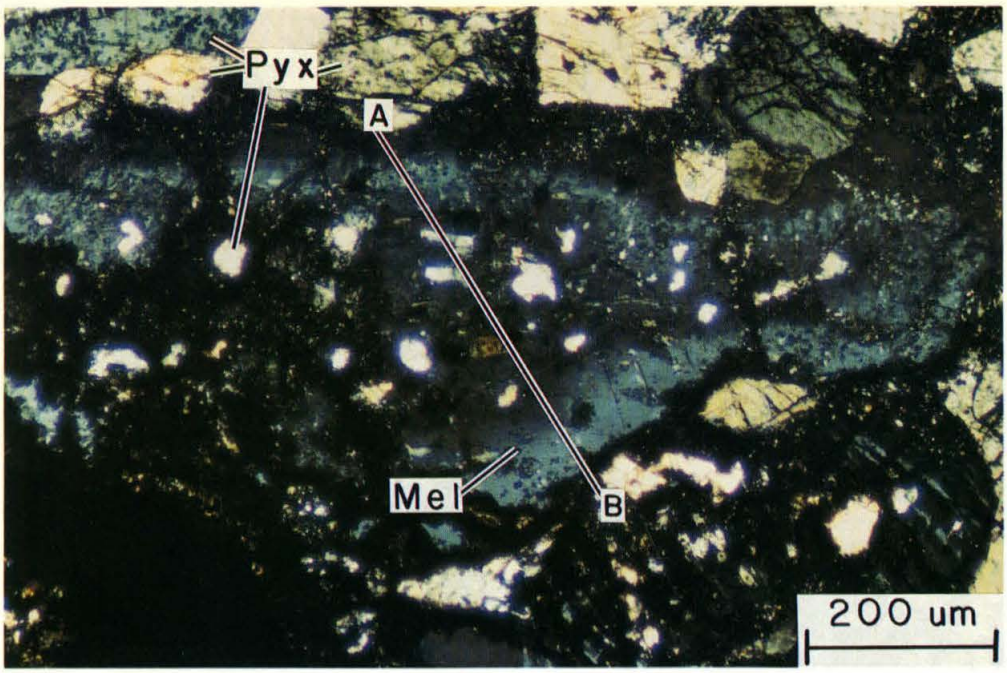

FIG. 3*a*.—Photomicrograph of a large melilite crystal in a Type B2 inclusion, TS21F1. The crystal is reversely-zoned from its core outwards, with only the outermost rim being normally-zoned. Pyroxene inclusions are abundant in the core of this melilite, just as in the similar crystal in figure 2*a*. Melilite core, Geh ~ 50, is nearly isotropic. Abbreviations as before.

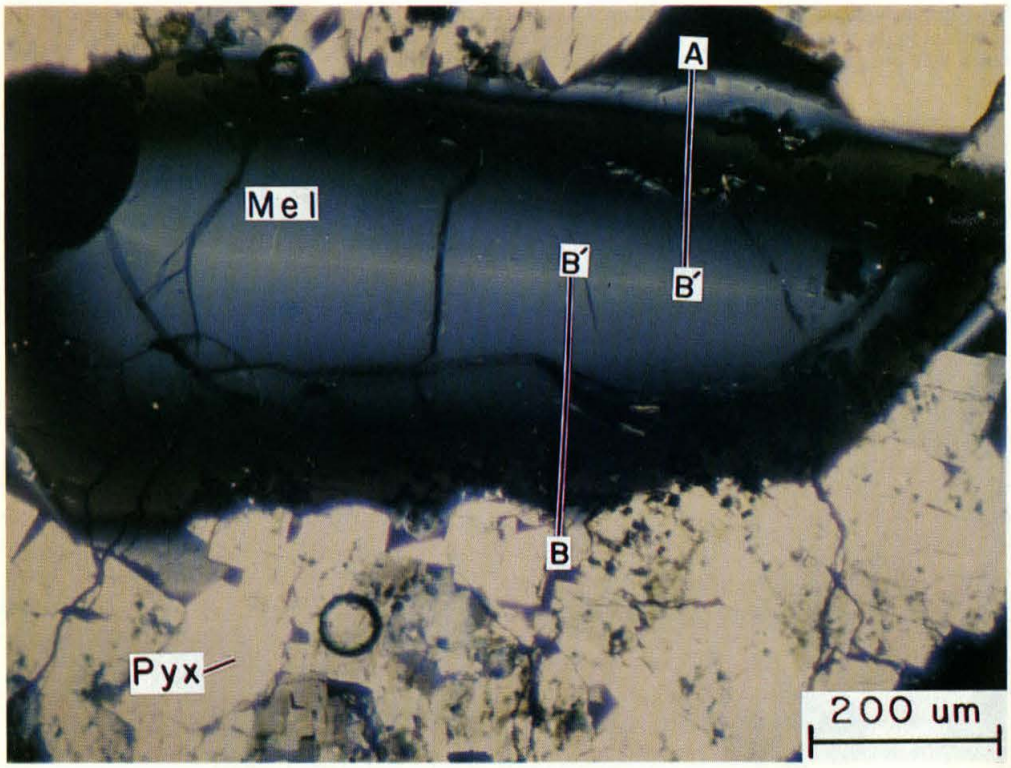

FIG. 4*a*.—Photomicrograph of a large melilite crystal produced during the experimental crystallization of a liquid having the approximate composition of a Type B1 inclusion. The cooling rate of this run was 2°C/hour. The crystal is normally-zoned from its core outwards, except for a reversely-zoned outermost rim. Unlike the natural samples, there is no normally-zoned outer rim. Note that neighboring pyroxene grains project into the melilite crystal no farther than the most Mg-rich (olive-brown) intermediate zone.

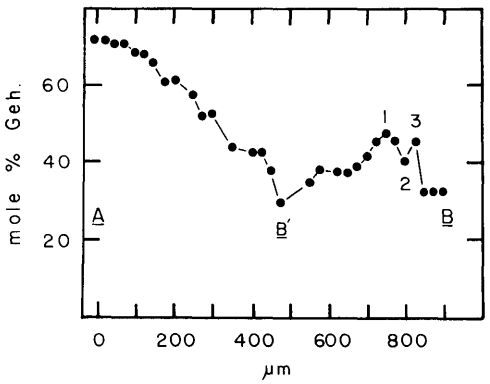

FIG. 1*b*.—Composition profile of crystal shown in figure 1*a*. The numbers 1–3 mark the positions where the step-scan crosses the correspondingly-numbered zones shown in figure 1*a*.

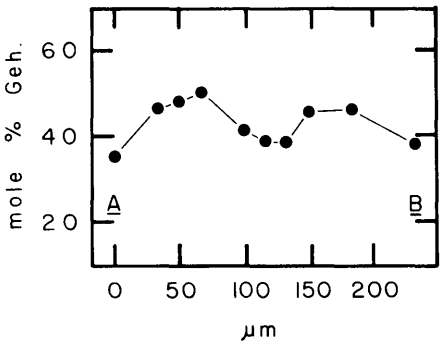

FIG. 2*b*.—Composition profile of crystal shown in figure 2*a*. This profile does not pass through the center of the melilite, owing to the abundance of pyroxene and spinel inclusions. The reverse zoning does extend into the true core, however, as analyses give a composition of Geh ~ 36 just to the left of the central pyroxene inclusion. Abbreviations as used previously.

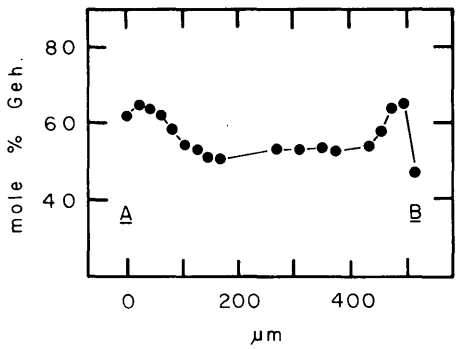

FIG. 3*b*.—Composition profile of the crystal shown in figure 3*a*. The core of the melilite, having a composition Geh ~ 50, is nearly isotropic. Abbreviations as used previously.

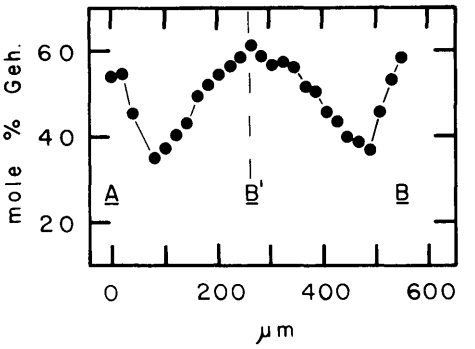

FIG. 4*b*.—Composition profile of the crystal shown in figure 4*a*. The vertical dashed line marks the discontinuity in the microprobe traverse as shown in figure 4*a*. Abbreviations as used previously.

an optical microscope because the birefringence of gehlenite-åkermanite solid solutions is a smooth and sensitive function of composition, particularly in the aluminum-rich part of the system (Osborn and Schairer 1941). An important feature of the melilite crystal in figure 1 is the spatial distribution of inclusions of pyroxene and spinel with respect to the melilite zoning. Spinel inclusions are scattered throughout the melilite, and mantling most of the spinel grains is a thin (≤5–10 μm) rim of brightly birefringent fassaite. These pyroxene rims are rare on spinel grains in the core of the melilite host, but their abundance and thickness increase abruptly in the åkermanite-rich zone just to the interior of where the reverse zoning first begins.

In contrast to this large and presumably early-formed melilite crystal in TS23F1, figure 2 shows that much smaller and presumably later-formed melilite crystals in the same inclusion exhibit reverse zoning from their cores outwards and not just in their rims. As in the large melilite crystals noted above, however, the very outermost rims of these small melilite crystals are normally-zoned. In these crystals, pyroxene inclusions are prominent even in the cores of the melilite.

Taken in combination, these textures suggest the following crystallization history for TS23F1. Spinel began crystallizing first, followed by melilite, and then by pyroxene. The pyroxene rims on some spinels suggest that either spinel reacted with the liquid to form pyroxene or pyroxene nucleated on the surfaces of spinel crystals. That the observed textures are not due to a spinel-melilite reac-

tion is shown by the occurrence of pyroxene rims on spinel enclosed within anorthite as well as within melilite (fig. 8). The melilite became steadily more åkermanite-rich with falling temperature, reaching a composition of Geh ~ 30 just prior to the first appearance of pyroxene. Immediately thereafter, the melilite started to become more *gehlenite*-rich. Anorthite was apparently the last phase to appear in the crystallization sequence, and started to crystallize at about the temperature at which the melilite reverse zoning reached its maximum gehlenite content. This conclusion is based on the fact that anorthite crystals project no farther into adjacent melilite crystals than the outer edge of the innermost reversed zone in the latter phase. After anorthite crystallization began, the melilite once again became more åkermanite-rich with progressive crystallization. A rare phenomenon, the second reversal seen in figure 1, will be discussed later.

Similar features are present in another Type B1, TS34F1, illustrated in its entirety in Clayton et al. (1977) in their figure 4. The elongate melilite crystals projecting inward from the inclusion margin are normally-zoned along their lengths toward the inclusion center. As in the inclusion described by MacPherson and Grossman (1981), these crystals are interpreted to be the first that nucleated during solidification of the droplet that formed the inclusion and to have grown inward with falling temperature. Smaller melilite crystals in the core of the inclusion nucleated later. Pyroxene rims on spinel enclosed within the elongate melilites become abundant near the inner ends of the melilite crystals, and a thin reversed zone, followed by a thin normal zone, is found at the innermost tips of these crystals. Melilite grains in the interior of TS34F1, where pyroxene is abundant, show reverse zoning on their rims only (large crystals) or in their cores (small crystals).

Some Type B2 inclusions contain only normally-zoned melilite crystals, some contain only reversely-zoned melilite and still other Type B2's contain both normally- and reversely-zoned crystals. In Type B2 inclusions, the reverse zoning, where present, occurs in the cores of the crystals, and only the outermost rims are normally-zoned. Figure 3 shows an example of a melilite crystal from the Type B2 inclusion designated TS21F1, along with a composition profile measured across it. The core of the melilite has a composition of Geh ~ 50 and has numerous pyroxene inclusions. The core is reversely-zoned, reaching Geh ~ 65 near the rim, and is mantled by a normally-zoned rim that reaches Geh ~ 47. Because of sectioning effects, however, we cannot rule out the possibility that some of these crystals may have small, normally-zoned cores.

Two general patterns emerge from the above observations. First, pyroxene inclusions within melilite are always most abundant in the åkermanite-rich zones just interior to where reverse zoning of the melilite begins: near the rims in B1 melilite crystals and in the cores of B2 melilite crystals. Second, reverse zoning begins only from a rather åkermanite-rich composition: Geh ~ 30 in the outer zones of B1 melilite and Geh ~ 50 in the cores of B2 melilite. We intend to show that, under certain conditions, co-precipitation of pyroxene and Mg-rich melilite drives up the Al/Mg ratio of the residual liquid and causes the growing melilite crystals to become reversely-zoned.

EXPERIMENTAL REPRODUCTION OF REVERSELY-ZONED MELILITE IN LIQUIDS OF TYPE B COMPOSITION

Liquids having the bulk composition of an "average Type B inclusion" (as given by Stolper 1982) were cooled from 1420°C to 1025°C at rates ranging from 0.5°C/hour to 1000°C/hour (Paque and Stolper 1983). This composition is similar to an average Type B1 inclusion and contains less normative pyroxene than most Type B2's. The equilibrium crystallization sequence of a liquid of this composition is spinel, melilite, anorthite, and finally fassaite. At all cooling rates studied, the order of appearance of anorthite and fassaite is reversed relative to the equilibrium case. Reversely-zoned melilite was produced in runs with cooling rates in the range 0.5–20°C/hour but was not observed in runs cooled at rates of 50°C/hour or more.

Figure 4 shows an example of one of the run products cooled at 2°C/hour from a maximum temperature of 1420°C and quenched at 1142°C. From the accompanying electron microprobe traverse, it is seen that the core of the melilite crystal has the composition of

Geh ~ 61 and is normally-zoned for about 60% of the crystal width to a composition of Geh ~ 37. From that point outward, the crystal is reversely-zoned, culminating in a rim composition of Geh ~ 63. Pyroxene grains bordering the melilite are partly enclosed within it but extend no farther into the melilite than to the most åkermanite-rich zone. Experimental charges cooled from 1420°C at 2°C/hour but quenched at temperatures of 1200°C or higher show only normally-zoned melilites and have no pyroxene crystals. Only experiments quenched at temperatures at or below 1185°C, the temperature at which fassaitic pyroxene is first found in experimental run products along with melilite at this cooling rate, have melilites with reversely-zoned rims. Thus, in our experiments, the reverse zoning of melilite coincides with and, as we shall show below, is probably the result of the onset of pyroxene + melilite (+ spinel) coprecipitation.

In runs with cooling rates ≥50°C/hour, the melilite is not reversely-zoned even though pyroxene crystallizes before anorthite. The reason may be that pyroxene that forms at higher cooling rates has higher Al_2O_3/MgO ratios than the coexisting liquid, while that which forms at lower cooling rates has lower Al_2O_3/MgO ratios than the liquid (Paque and Stolper 1983). Thus, when pyroxene crystallizes at high cooling rates, the Al_2O_3/MgO ratio of the liquid falls and normally-zoned melilite continues to grow. At lower cooling rates, the Al_2O_3/MgO ratio of the liquid rises and reversely-zoned melilite forms when pyroxene appears.

The experimental run products differ from natural Type B's in two respects. First, none of the experiments produced a normally-zoned outermost rim overlying the reversely-zoned interval on the melilite crystals, whereas such a rim is present on nearly all natural Type B melilite. Second, experimental run products containing both pyroxene and anorthite sometimes have reversely-zoned melilite and sometimes do not, even though the experiments were run under identical conditions. As discussed below, these differences may be related to the random nature of anorthite nucleation (e.g., Gibb 1974) so that, in some experiments, anorthite begins crystallizing before pyroxene at slow cooling rates, producing melilites with only normal zoning, whereas, in other experiments run at the same cooling rates, pyroxene begins crystallizing first and reversely-zoned melilites result.

DISCUSSION

Origin of Reverse Zoning in Melilite.—Gee and Osborn (1969, p. 36–39) predicted that a variety of zoning patterns, including single and double reversals, are possible for melilites crystallizing from bulk compositions falling in the system gehlenite-åkermanite-diopside-anorthite, the details depending on the bulk composition. Figure 5, which shows spinel-saturated phase equilibria in the system CaO-MgO-Al_2O_3-$SiO_2(-TiO_2)$, can be used to explain why reverse zoning occurs in our experimental charges and, by analogy, in naturally occurring Type B melilites. The diagram is after Stolper (1982), but the fields have been distorted for illustrative purposes. Composition *A* is representative of a typical Type B1 inclusion composition. *Aab* illustrates the path of liquid compositions followed during equilibrium crystallization of composition *A*. As the liquid composition changes from *A* to *a*, spinel and melilite are the only phases crystallizing, and the melilite composition becomes continuously more åkermanitic as the temperature falls. At *a*, anorthite joins the crystallization sequence, the residual liquid moves from *a* to *b* and the melilite continues to become more åkermanitic as the normative gehlenite/åkermanite ratio of the liquid continues to decrease. At *b*, pyroxene joins the crystallization sequence and the melilite composition remains constant as the liquid is consumed in the reaction sp + liquid = mel + an + cpx.

Consider now the fractional crystallization of composition *A* as a model for understanding the results of our dynamic crystallization experiments. The residual liquids now follow a shallower curved path such as *Ac* across the melilite field to the edge of the anorthite field at *c*, and the melilites are normally-zoned. If nucleation sites for anorthite were available under the conditions of the experiment, anorthite would begin to crystallize at this point and the residual liquid would move down the anorthite + melilite + spinel cotectic from *c* to *b*, at which point pyroxene would crystallize if nucleation sites were available. The melilites would be normally-

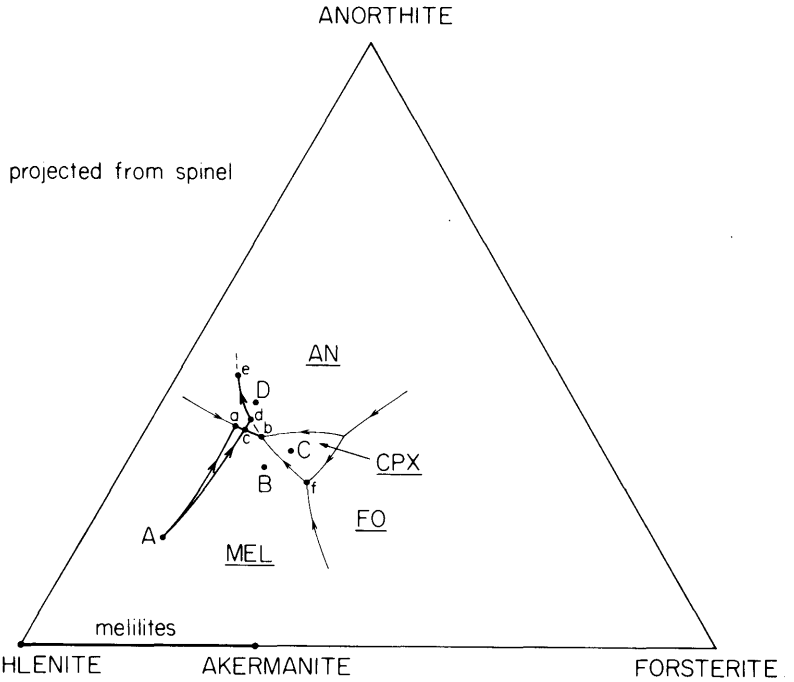

FIG. 5.—Spinel-saturated liquidus diagram for the system CaO-MgO-Al_2O_3-SiO_2(−TiO_2), projected onto the plane anorthite-gehlenite-forsterite, for compositions having $TiO_2 \leq 5$ wt%. The fields have been distorted in order to better show possible crystallization paths for liquids of Type B composition. See text for discussion.

zoned in this case. If, however, anorthite fails to nucleate at *c*, as is the case under all but the slowest of cooling rates, the liquid will continue past the stable anorthite + melilite + spinel cotectic, metastably precipitating normally-zoned melilite + spinel as the liquid continues on the path *c* to *d*. At *d*, the liquid encounters the metastable extension of the pyroxene + melilite + spinel cotectic. If nucleation sites are available, pyroxene will begin to precipitate at this point and the liquid will move along the metastable cotectic from *d* in the direction of *e*. Along this part of the crystallization sequence, the melilites can be expected to be reversely-zoned. This is due to the fact that as the liquid composition moves to the left on this figure, as it does between *d* and *e*, the normative gehlenite/åkermanite ratio of the liquid increases (i.e., the Al/Mg ratio increases) and so too will the gehlenite content of the crystallizing melilite. Evidence that this indeed occurred in our experiments is provided by figure 6, which shows the Al/Mg ratios of the glasses and the compositions of the outermost edges of the coexisting melilite crystals as a function of quench temperature in the experiments in which the cooling rate was 2°C/hour. Prior to pyroxene precipitation, the Al/Mg ratio of the liquid changes little as the gehlenite contents of the edges of the melilite grains gradually decrease with falling temperature. Once pyroxene begins to crystallize at 1185 ± 15°C, however, the Al/Mg ratio increases dramatically, and the outer edges of the melilite crystals become much more gehlenitic with a further, relatively small, temperature decline. Figure 6 shows clearly that the zoning reversal in the melilite is correlated with the Al/Mg ratio of the liquid which, in turn, is strongly affected by pyroxene crystallization. There is a suggestion in the natural inclusions described above, however, that reverse zoning did not begin immediately upon the first appearance of pyroxene but, rather, shortly thereafter. Perhaps this has something to do with the amount of pyroxene that crystallizes. When pyroxene first precipitates, the amount may be so small that its effect on the liquid composition is insufficient to have a

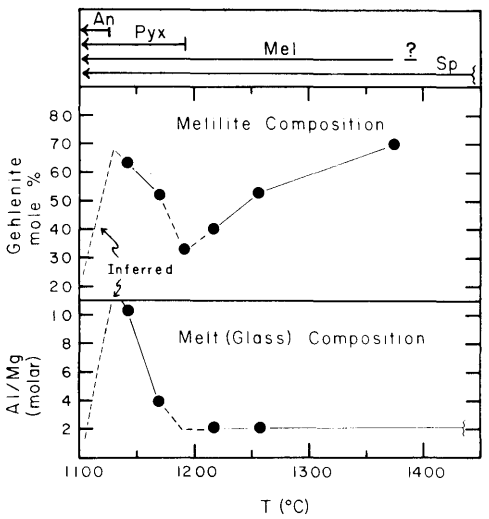

FIG. 6.—Compositions of melilite rims and their co-existing liquids (= quenched glasses) in our experimental runs, plotted as a function of the quench temperature of the respective runs. All data shown are from runs cooled at 2°C/hour. The crystallization sequence is shown at top. The inflections in the dashed lines mark the approximate temperatures at which pyroxene and anorthite first begin to crystallize. The melilite composition shown at 1185°C is inferred from the most magnesium-rich melilite observed in the 1160°C run. The gehlenite content of the melilite parallels the Al/Mg ratio of the liquid, and both increase sharply with falling temperature immediately following the onset of clinopyroxene precipitation. The dashed lines below 1140°C are inferred from runs containing anorthite and in which the melilite crystals do not show reverse zoning. Sp—spinel. Other abbreviations as used previously.

large impact on the composition of the precipitating melilite. Only as more pyroxene crystallizes does it have a significant effect on melt composition. At some point, as the residual liquid moves from *d* toward *e*, anorthite may begin to crystallize (e.g., at ~1120 ± 20°C on fig. 6). When it does, the liquid composition might be expected, barring kinetic constraints, to move back toward the temperature and composition of the unique, stable liquid in equilibrium with spinel + mel + cpx + an; i.e., toward *b*. The details of what might happen are difficult to specify, but we may expect resorption of some pyroxene and melilite and precipitation of more åkermanitic melilites of the sort that are in equilibrium with liquids in the vicinity of *b* (as opposed to those in equilibrium with liquids from *d* to *e*).

Figure 5 thus provides a relatively simple rationale for understanding the zoning patterns of melilites in Type B1 inclusions. Normally-zoned melilites are precipitated initially, as long as spinel and melilite precipitate alone ($A \rightarrow d$); reversely-zoned melilites then grow as pyroxene joins the crystallization sequence ($d \rightarrow e$); finally, partial resorption of the reversed zone and overgrowth of normally-zoned melilites can be expected as anorthite joins the crystallization sequence ($e \rightarrow \sim b$).

Figure 5 is, in some respects, an oversimplified representation of the phase equilibria needed to understand the evolution of Type B inclusions under non-equilibrium conditions. The appearance of pyroxene, like that of anorthite but to a lesser extent (Grove and Bence 1979; Paque and Stolper 1983), is suppressed at rapid cooling rates. Thus, even when the liquid reaches the composition *d* on the metastable equilibrium sp + mel + cpx cotectic, pyroxene will not begin to crystallize immediately. Spinel and melilite will continue to precipitate alone, and the residual liquid will continue along the extension of the curve *Acd* until pyroxene finally begins to crystallize. When this happens, there will be a tendency for the liquid to move back toward the curve *de*. Since, however, the composition of the crystallizing pyroxene will be a function of cooling rate and bulk composition of the liquid, and will be spatially heterogeneous, the actual location of the metastable sp + mel + cpx cotectic along which the liquids will evolve is not unique or as simple as the curve *bde* in figure 5 would suggest. Indeed, at rapid cooling rates, the pyroxenes show a tendency toward higher Al/Mg ratios than do pyroxenes formed at slower cooling rates. Under these conditions, the residual liquids may move to the *right* in figure 5 with decreasing temperature as sp + mel + cpx crystallize. This may be why reversely-zoned melilites are not found in experiments with cooling rates $\geq$50°C/hour.

It is important to emphasize that the reverse zoning is, according to our interpretation, a consequence of the co-precipitation of melilite and clinopyroxene in the absence of anorthite precipitation, and thus that the observation of this feature gives information on the crystallization sequence followed by a particular inclusion. In most of our dynamic

crystallization experiments on the average Type B1 composition, pyroxene crystallized before anorthite because anorthite precipitation was delayed. At slow cooling rates (0.5 and 2.0°C/hour), however, anorthite precipitation was not always suppressed relative to pyroxene. Therefore, at these cooling rates, reverse zoning was not always observed in melilites crystallized from this bulk composition, its occurrence depending on the order of anorthite and pyroxene crystallization in each individual experimental charge. Because of the random nature of anorthite nucleation, there does not exist a critical cooling rate at which pyroxene and anorthite would begin simultaneously to crystallize from this composition. Rather, there exists a range of cooling rates within which either reversely- or normally-zoned melilite would be expected in different samples with the same bulk composition and under the same experimental conditions. At slower cooling rates, the proportion of samples with reversely-zoned melilite decreases since, under these conditions, anorthite becomes more likely to precede pyroxene in the crystallization sequence. It is inferred that at some particular cooling rate, <0.5°C/hour, anorthite will crystallize before pyroxene in nearly all cases and that this would represent an approximate lower limit for the cooling rates of natural inclusions with reversely-zoned melilite, provided, of course, that the nucleation behavior of anorthite in Allende inclusions was similar to that in our experiments. An upper limit for the cooling rates of natural inclusions of ~50°C/hour can be deduced from the fact that in our experiments conducted at this cooling rate and faster, reverse zoning was not observed in melilites. Perhaps, as suggested above, this is due to the dependence of pyroxene composition on cooling rate.

The reason why pyroxene crystallizes prior to anorthite in the average Type B1 composition shown in figure 5 is that anorthite crystallization is suppressed to a temperature lower than that of the onset of pyroxene crystallization. Other compositions can be expected to exhibit melilites with reverse zoning even in the absence of these kinetic factors. For example, a composition such as *B* would crystallize melilite followed by pyroxene under conditions of both equilibrium and fractional crystallization. Thus, a normally-zoned melilite core overgrown by a reversely-zoned region would be expected for all but perhaps the very fastest cooling rates. A normally-zoned rim resulting from the entry of anorthite into the crystallization sequence would also probably form in this case. A composition such as *C* would crystallize pyroxene prior to melilite under conditions of equilibrium and fractional crystallization, and the melilite would have a reversely-zoned core and probably a normally-zoned rim resulting from the entry of anorthite into the crystallization sequence. Some compositions in the melilite field would crystallize melilite followed by anorthite under equilibrium conditions, but would crystallize melilite followed by pyroxene during fractional crystallization. The latter case would not be because of the difficulty of anorthite nucleation as for composition *A*, but because the residual liquid path during fractional crystallization intersects the curve *bf* rather than *ab* (Stolper 1982). Composition *d* on figure 2-9 of Gee and Osborn (1969) exhibits this type of behavior and, under conditions of fractional crystallization, would produce melilite with a normally-zoned core and a reversely-zoned rim.

Some Type B2 inclusions have bulk compositions that can be represented schematically by point *D* (Stolper 1982). Under equilibrium conditions, anorthite would precipitate first but, at all except very slow cooling rates ($\lesssim$ a few degrees per hour), clinopyroxene would probably crystallize first, followed by melilite when the residual liquid reaches the curve *fdbe*. Melilite with reversely-zoned cores would thus result. These would probably have normally-zoned rims, reflecting the entry of anorthite later in the crystallization sequence. Melilite with such zoning patterns is seen in many Type B2 inclusions. Some Type B2 compositions fall inside the melilite field, however, and melilites with normally-zoned cores and reversely-zoned rims would be expected. Because the compositions of these Type B2 inclusions lie closer to the anorthite boundary than Type B1 compositions, less melilite will crystallize prior to pyroxene entry in B2's than in B1's. This would be expected to lead to melilite crystals in Type B2's in which the reversely-zoned mantles are thicker in comparison to the normally-zoned cores than in the B1's. In those Type B2 inclusions that

contain melilite crystals with normally-zoned cores, however, reversely-zoned rims have not been observed. Because these inclusions contain none of the textural or other mineral chemical characteristics found in the experiments conducted at fast cooling rates (Paque and Stolper 1983), they probably did not cool more quickly than those containing reversely-zoned melilite. It may be that these inclusions cooled more slowly than the latter or that more favorable sites were available for anorthite nucleation, such that anorthite crystallization began before pyroxene crystallization. We have also seen one Type B2 inclusion in which almost all of the melilite crystals are normally-zoned from core to rim, but one crystal is entirely reversely-zoned, for which we have no explanation. We note that this cannot be a sectioning effect, as no other crystals show reversely-zoned rims.

One Type B1 inclusion was seen in which many of the melilite crystals have a normally-zoned core, then a relatively thin reversed zone, then a normal zone, then another reversed zone followed by an outer normal zone. One such crystal is illustrated in figure 1. Although the origin of oscillatory zoning in igneous rocks is, in general, poorly understood, it is conceivable that its presence in the melilite of this inclusion records fluctuations in the temperature or cooling rate of the environment in which this inclusion formed.

Available phase equilibria thus provide a relatively simple framework for understanding the occurrence of reversely-zoned melilites in Type B inclusions in Allende. The co-precipitation of melilite and pyroxene without anorthite is the principal requirement for production of this feature. Kinetic and/or compositional factors may be responsible for crystallization of pyroxene prior to plagioclase, which leads to this zoning pattern. The different zoning patterns in melilites from Types B1 and B2 inclusions are easily understood in light of compositional differences between these two classes of inclusion.

Cooling Rates of Type B1 Inclusions.—As discussed above, our experiments indicate that typical Type B1 inclusions with reversely-zoned melilites probably cooled through the temperature interval ~1420°C–1000°C at a rate of <50°C/hour. No firm lower limit on the cooling rate of such inclusions has been established because we have not determined the cooling rate at which plagioclase nearly always begins to precipitate before pyroxene. Based on the present experimental data, the lower limit is probably <0.5°C/hour, assuming that the nucleation behavior of anorthite in Allende inclusions was similar to that in our experiments. Other aspects of Type B1 textures and phase chemistry also suggest that cooling rates on this order are involved in the formation of these inclusions (Paque and Stolper 1983). In addition, Paque and Stolper (1983) conclude, based on dynamic crystallization experiments, that most Type B inclusions began the cooling sequence that led to their observed textures from below their liquidi; i.e., most inclusions were never totally molten.

The inferred cooling rates are surprising because they are too low for small droplets that presumably cooled by radiation in the low pressure ($P_t \leq 10^{-3}$ atm) environment of the solar nebula. As shown by Tsuchiyama et al. (1980), the cooling rate of a radiating liquid spherule is given approximately by

$$\frac{dT}{dt} = \frac{-3\,\epsilon\,\sigma}{r\rho\left(C_p + \frac{\Delta H_c}{\Delta T_c}\right)}\,(T^4 - T_o^4) \quad (1)$$

where T and T_o are the absolute temperatures of the spherule and its surroundings, respectively, σ is the Stefan-Boltzmann constant (5.7×10^{-12} J · cm^{-2} · sec^{-1} · °K^{-4}), ρ and C_p are the liquid density and heat capacity, respectively, ΔH_c is the latent heat of crystallization, ΔT_c is the temperature interval over which crystallization occurs and ϵ and r are the emissivity and radius of the spherule, respectively. Consider as an example a molten spherule having the Type B1 composition used in our experiments, with r ~ 0.25cm, C_p ~ 1.5 J · g^{-1} · °K^{-1} (estimated from data of Carmichael et al. 1977), ρ ~ 2.8 g · cm^{-3} (calculated by the method of Bottinga and Weill 1970), ϵ ~ 0.8 (Carslaw and Jaeger 1959), and cooling through the temperature range of melilite crystallization (1723°K to 1373°K). ΔH_c for spinel and melilite are not known, but for anorthite and diopside the values are ~487 J/g (Weill et al. 1980) and 638 J/g (Stebbins et al. 1983), respectively. Accordingly, we assume the approximate value of 550 J/g for the average ΔH_c of the entire molten droplet. If the temperature of the ambient gas is

taken as 1373°K, the solidus temperature of the liquid, the cooling rate from (1) above is ~33°K/sec. This is three orders of magnitude greater than the cooling rates inferred from our experiments for Type B1 inclusions that exhibit reverse zoning. Even if the temperature of the ambient gas were 1722°K, only 1° below the temperature of first appearance of melilite, the cooling rate over this 1°K temperature interval would still be in excess of 460°K/hour, after which the liquid cooling rate would be controlled by the gas cooling rate. Such a discrepancy between calculated and experimentally determined cooling rates was also noted in the case of olivine chondrules (Tsuchiyama et al. 1980).

A small droplet immersed in a hydrogen gas simply cannot be insulated sufficiently to cause it to cool at rates significantly slower than those above unless it is closely surrounded by a densely packed population of other hot solid or liquid objects. In the absence of heat sources, it is likely instead that the Type B1 inclusions had the same temperature and cooled at the same rate as their surrounding gas. The time scale for cooling of the solar nebular cloud is thought to be on the order of at least 10^4 years (Clark et al. 1972; Cameron 1978). Although we have not determined the lower limit to the cooling rate required to produce reverse zoning in melilite, it is very likely that the cooling rate of the nebula, $\sim 10^{-5}$°K/hour, is far too slow to suppress plagioclase crystallization significantly and result in reversely-zoned melilite in Type B1 inclusions. One possibility is that the droplets cooled more rapidly than the nebula as a whole, inside small hot regions that existed within the larger and cooler nebular cloud. Alternatively, the cooling rate could have been controlled by the velocity of the droplets as they were transported from hot regions of the nebula to cooler ones.

Other mechanisms for retarding the rate of cooling involve heat sources. One example might be the early sun, if it had ignited by the time these inclusions formed (Wasserburg and Papanastassiou 1982). Another possible heat source might have been friction due to the effects of drag as inclusions moved rapidly through the nebular gas, such as in the model suggested by Wood (1983).

Comments on the Growth of Melilite in Type B Inclusions.—Meeker et al. (1982, 1983*a*, 1983*b*) described grains of fassaite within melilite in several Type B inclusions and gave textural arguments that the melilite formed by metamorphic replacement of pyroxene. We show here that the textural relationships between most of the melilites and pyroxenes that we have observed are explicable in terms of crystallization of both phases from a melt and consistent with the interpretation we have presented above for the origin of zoning patterns in Allende melilite.

Our examination of Type B's indicates that there are three textural varieties of pyroxene inclusions in melilite. The first occurs as rims on spinel grains (fig. 7). Commonly, one poikilitic pyroxene grain will enclose a cluster of spinel grains. In some cases, these pyroxene grains are in optical continuity with one another. Similar pyroxene rims around spinel inclusions are found inside anorthite crystals, such as the one shown in figure 8. A logical extension of the metamorphic replacement model would have to be that anorthite, as well as melilite, formed by replacement of pyroxene. Within melilite, the abundance of these pyroxene inclusions is greatest in the magnesium-rich zones of reversely-zoned crystals, consistent with our interpretation that the onset of pyroxene precipitation from a melt coincided with the onset of reverse zoning in co-crystallizing melilite. Our interpretation of pyroxene inclusions within both melilite and anorthite is simply that pyroxene was incorporated by growing melilite and anorthite during their crystallization from a liquid.

A second variety of pyroxene inclusion in melilite occurs as tiny (5–40 μm long, <5 μm wide) blades that are oriented parallel to the c-axis of the host melilite (fig. 9). These have been found in some compact Type A inclusions (MacPherson and Grossman 1979) as well as in some Type B's. The small size, euhedral shape, and crystallographic orientation of these pyroxene crystals within their host suggest they formed by exsolution from the melilite.

The third kind of pyroxene inclusion occurs as rounded to irregularly-shaped crystals that can be moderately large (up to ~500 μm) and do not form rims on spinel crystals. This is the kind of pyroxene inclusion described by Meeker et al. (1983*b*). These are very common in the reversely-zoned cores of meli-

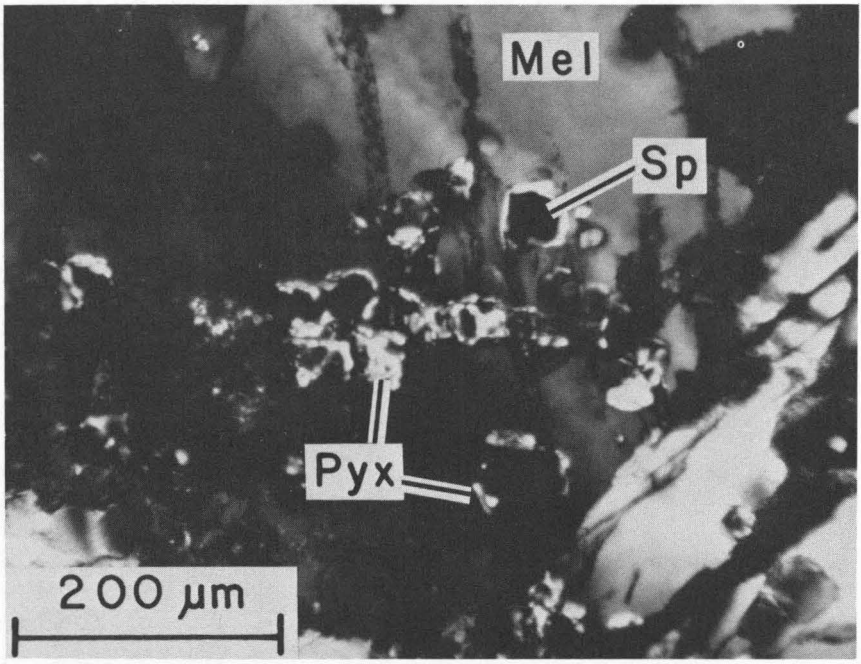

FIG. 7.—Photomicrograph of spinel grains (isotropic) having thin clinopyroxene rims (brightly birefringent), both being enclosed within melilite (at extinction) in the Type B1 inclusion TS34F1. Photograph taken in transmitted light, with crossed polarizers. Abbreviations as used previously.

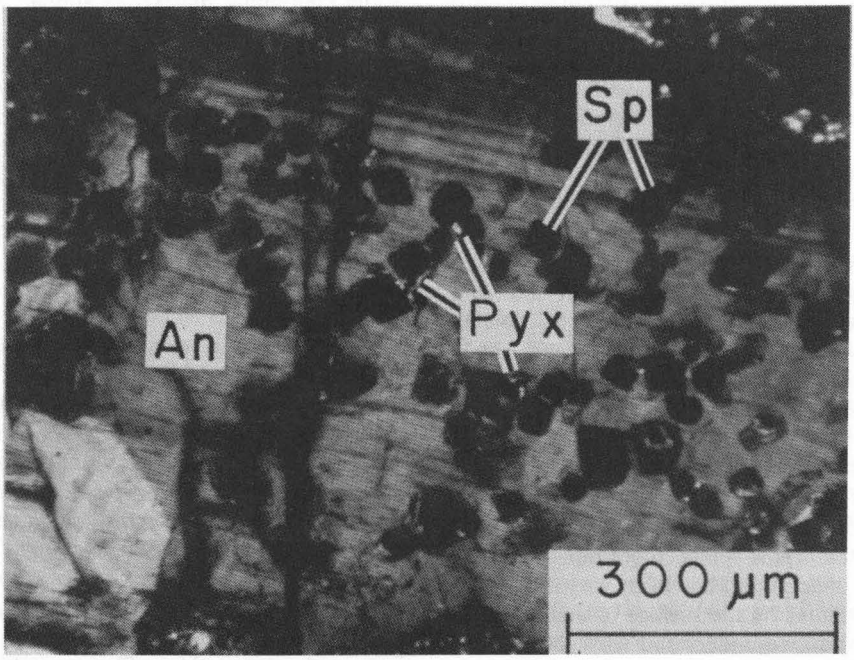

FIG. 8.—Photomicrograph of spinel grains (isotropic) having thin clinopyroxene rims (bright), both being contained within a large twinned anorthite crystal in a Type B1 inclusion. Photograph taken in transmitted light, with crossed polarizers. Abbreviations as used previously.

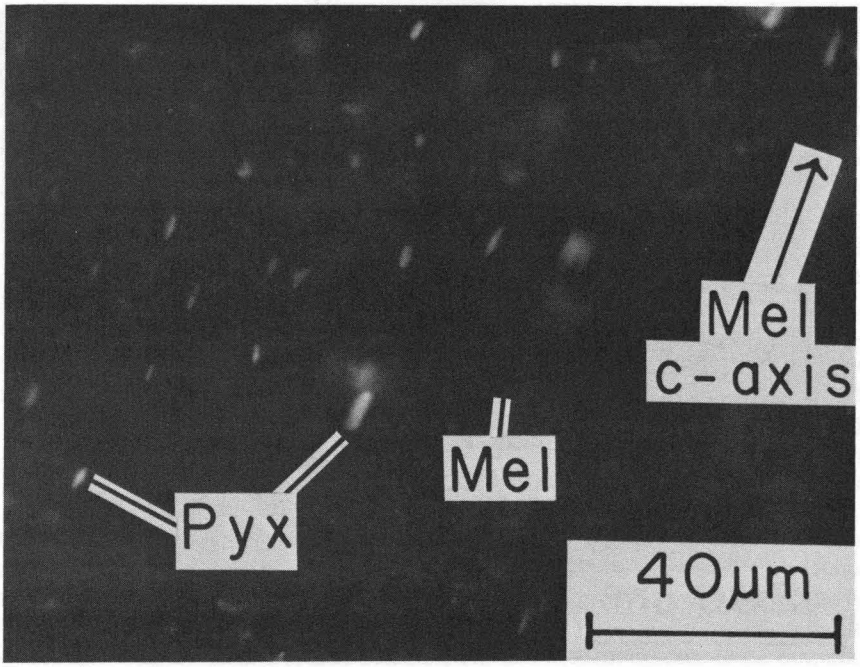

FIG. 9.—Photomicrograph of tiny blades of birefringent clinopyroxene, enclosed within melilite (at extinction), and having their long axes parallel to the c-axis of the host melilite crystal. Photograph taken in transmitted light, with crossed polarizers. Abbreviations as used previously.

lite crystals in B2's but almost never occur in the gehlenite-rich cores of B1 melilite. Figure 10 shows pyroxene grains within a single, zoned melilite crystal in a Type B1. Several grains are roughly equant with irregular or scalloped outer margins. The most important feature in this photo is the arcuate pyroxene band. It is completely enclosed by the same melilite crystal and its shape is precisely concentric with the melilite composition contours, suggesting that the pyroxene formed during growth of the melilite by nucleating on and coating part of the surface of the growing crystal. The pyroxene in this arc is a single crystal that *is in optical continuity with some of the irregular pyroxenes noted above and shown nearby in the photo*. These observations suggest to us that these pyroxenes also formed during growth of the melilite rather than prior to it, which would be required by the metamorphic replacement model. We do not yet understand, however, why the pyroxene nucleates on the surface of melilite crystals, nor do we understand why some of the natural pyroxene has a scalloped appearance.

In summary, textural and experimental evidence suggest to us an igneous origin for most melilites in Type B inclusions, including some containing pyroxenes similar to those described by Meeker et al. (1982, 1983*a*, 1983*b*) and suggested by them as due to metamorphic replacement of pyroxene. Although we cannot rule out a metamorphic origin for some melilite in some refractory inclusions, we feel that those we have studied here are more compatible with an igneous origin.

CONCLUSION

Melilites in many Type B Ca-, Al-rich inclusions from the Allende meteorite are not simply "normally-zoned" from gehlenite-rich cores to åkermanite-rich rims. Type B1 melilites often have normally-zoned cores, overgrown by a reversely-zoned region which is, in turn, enclosed within a normally-zoned rim. Our petrographic observations on Type B inclusions and our dynamic crystallization experiments on an average Type B1 composition suggest that reverse zoning in melilites is a direct consequence of the co-precipitation of spinel + melilite + pyroxene, without anorthite. The normally-zoned cores of Type B1 melilites formed during spinel + melilite precipitation; the reversely-

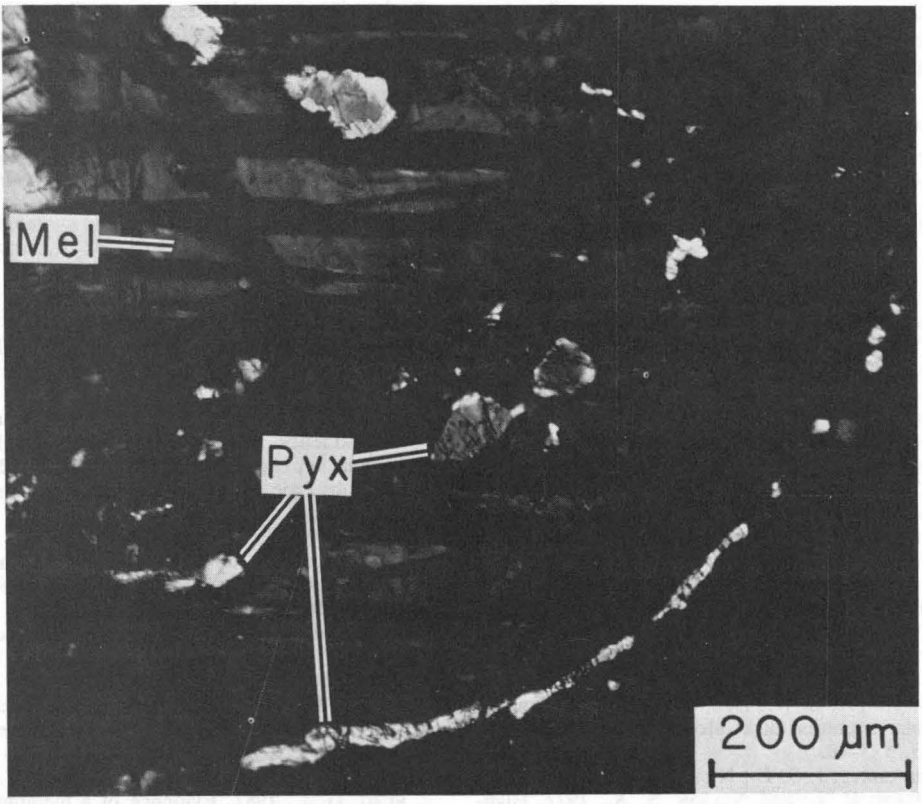

FIG. 10.—Photomicrograph of clinopyroxene grains enclosed within melilite in the Type B1 inclusion TS34F1. The arcuate band of pyroxene is a single crystal whose shape parallels the zoning contours (= birefringence contours) of the host melilite. Several of the irregular pyroxene grains near the top of the photo are in optical continuity with the arcuate pyroxene. Abbreviations as used previously.

zoned regions reflect the onset of pyroxene crystallization; and the normally-zoned rims formed when anorthite finally joined the crystallization sequence. The absence of a substantial normally-zoned core in most melilites from Type B2 inclusions reflects the difference in bulk composition between Types B1 and B2 inclusions: Type B2 inclusion compositions do not have a substantial interval over which spinel and melilite crystallize without pyroxene.

There are undoubtedly many modes of origin of melilites found in Ca-, Al-rich inclusions. We propose, however, that Type B melilites exhibiting the zoning patterns that we have described can be confidently ascribed to crystallization from a melt. This is based on their petrographic setting, the correlation between the nature of the zoning and the bulk compositions of the inclusions (i.e., Type B1 vs. Type B2) and the fact that these features have been reproduced in dynamic crystallization experiments.

The crystallization of pyroxene plus melilite prior to anorthite precipitation, which is required to produce reversely-zoned melilites, may reflect bulk compositional and/or kinetic factors. In Type B1 inclusions, kinetic factors resulted in the suppression of anorthite crystallization relative to pyroxene and allowed an interval of spinel + melilite + pyroxene crystallization. Reversely-zoned melilites can only be produced from Type B1 compositions over a restricted range of slow cooling rates (<50°C/hour). Such cooling rates are far too slow to be explained easily in the context of radiative heat loss from molten droplets in a low pressure nebular environment. They probably reflect either the cooling rates of local regions of the nebular gas

itself or the influence of some heat source such as the sun or viscous drag on inclusions as they moved through the nebular gas.

ACKNOWLEDGMENTS.—We thank E. Anders, S. P. Clark, Jr., R. N. Clayton, R. J. Kirkpatrick, R. Lewis, D. Mackenzie, and F. Richter for helpful discussions. This research was supported by NASA Grants NGR 14-001-249 and NAG 9-54 (both to L. G.), NAGW-257 (E. S.) and NSF Grant EAR 821-8154 (L. G.). CIT Division of Geological and Planetary Sciences Contribution Number 4037.

REFERENCES CITED

ALLEN, J. M., and GROSSMAN, L., 1978, Solar nebula condensation: implications from Allende inclusion mineralogy (abs.): Meteoritics, v. 13, p. 383–384.

———; GROSSMAN, L.; DAVIS, A. M.; and HUTCHEON, I. D., 1978, Mineralogy, textures, and mode of formation of a hibonite-bearing Allende inclusion: Proc. 9th Lunar Planet. Sci. Conf., p. 1209–1233.

BLANDER, M., and FUCHS, L. H., 1975, Calcium-aluminum-rich inclusions in the Allende meteorite: evidence for a liquid origin: Geochim. Cosmochim. Acta, v. 39, p. 1605–1619.

BOTTINGA, Y., and WEILL, D. F., 1970, Densities of liquid silicate systems calculated from partial molar volumes of oxide components: Am. Jour. Sci., v. 269, p. 169–182.

CAMERON, A. G. W., 1978, Physics of the primitive solar accretion disk: Moon and the Planets, v. 18, p. 5–40.

CARMICHAEL, I. S. E.; NICHOLLS, J.; SPERA, F. J.; WOOD, B. J.; and NELSON, S. A., 1977, High-temperature properties of silicate liquids: applications to the equilibration and ascent of basic magma: Royal Soc. (London) Phil. Trans. A, v. 286, p. 373–431.

CARSLAW, H. S., and JAEGER, J. C., 1959, Conduction of Heat in Solids (2d ed.): London, Oxford University Press, 510 p.

CLARK, S. P., JR.; TUREKIAN, K. K.; and GROSSMAN, L., 1972, Model for the early history of the earth, *in* ROBERTSON, E. C., ed., The Nature of the Solid Earth: New York, McGraw-Hill, p. 3–18.

CLAYTON, R. N.; ONUMA, N.; GROSSMAN, L.; and MAYEDA, T. K., 1977, Distribution of the presolar component in Allende and other carbonaceous chondrites: Earth Planet. Sci. Letters, v. 34, p. 209–224.

EL GORESY, A.; NAGEL, K.; and RAMDOHR, P., 1979, Spinel framboids and fremdlinge in Allende inclusions: possible sequential markers in the early history of the solar system: Proc. 10th Lunar Planet. Sci. Conf., p. 833–855.

GEE, K. H., and OSBORN, E. F., 1969, Phase equilibria at liquidus temperatures in a part of the system CaO-MgO-Al_2O_3-SiO_2: the system $Ca_2MgSi_2O_7$ - $Ca_2Al_2SiO_7$ - $CaMgSi_2O_6$ - $CaAl_2Si_2O_8$: Penn. State Univ. Earth Min. Sci. Exper. Station Bull. 85, p. 23–51.

GIBB, F. G. F., 1974, Supercooling and crystallization of plagioclase from a basaltic magma: Mineral. Mag., v. 39, p. 641–653.

GROSSMAN, L., 1975, Petrography and mineral chemistry of Ca-rich inclusions in the Allende meteorite: Geochim. Cosmochim. Acta, v. 39, p. 433–454.

——— 1980, Refractory inclusions in the Allende meteorite: Ann. Rev. Earth Planet. Sci., v. 8, p. 559–608.

GROVE, T. L., and BENCE, A. E., 1979, Crystallization kinetics in a multiply saturated basalt magma: an experimental study of Luna 24 ferrobasalt: Proc. 10th Lunar Planet. Sci. Conf., p. 439–478.

MACPHERSON, G. J., and GROSSMAN, L., 1979, Melted and non-melted coarse-grained Ca-, Al-rich inclusions in Allende (abs.): Meteoritics, v. 14, p. 479–480.

———, and ——— 1981, A once-molten, coarse-grained, Ca-rich inclusion in Allende: Earth Planet. Sci. Letters, v. 52, p. 16–24.

———, and ——— 1984, "Fluffy" Type A Ca-, Al-rich inclusions in the Allende meteorite: Geochim. Cosmochim. Acta, v. 48, p. 29–46.

MEEKER, G. P.; ARMSTRONG, J. T.; and WASSERBURG, G. J., 1982, Evidence of a metamorphic origin for melilite in Allende CAI (abs.): Lunar Planet. Sci., v. 13, p. 505–506.

———; ———; and ——— 1983*a*, Petrography of WA, a well-known CAI from the Allende meteorite (abs.): Lunar Planet. Sci., v. 14, p. 493–494.

———; WASSERBURG, G. J.; and ARMSTRONG, J. T., 1983*b*, Replacement textures in CAI and implications regarding planetary metamorphism: Geochim. Cosmochim. Acta, v. 47, p. 707–721.

OSBORN, E. F., and SCHAIRER, J. F., 1941, The ternary system pseudowollastonite-akermanite-gehlenite: Am. Jour. Sci., v. 239, p. 715–763.

PAQUE, J. M., and STOLPER, E., 1983, Experimental evidence for slow cooling of Type B CAI's from a partially molten state (abs.): Lunar Planet. Sci., v. 14, p. 596–597.

STEBBINS, J. F.; CARMICHAEL, I. S. E.; and WEILL, D. F., 1983, The high temperature liquid and glass heat contents and the heats of fusion of diopside, albite, sanidine, and nepheline: Am. Mineral., v. 68, p. 717–730.

STOLPER, E., 1982, Crystallization sequences of Ca-Al-rich inclusions from Allende: an experimental study: Geochim. Cosmochim. Acta, v. 46, p. 2159–2180.

TSUCHIYAMA, A.; NAGAHARA, H.; and KUSHIRO, I., 1980, Experimental reproduction of textures of chondrules: Earth Planet. Sci. Letters, v. 48, p. 155–165.

WARK, D. A., and LOVERING, J. F., 1977, Marker events in the early evolution of the solar system:

evidence from rims on Ca-Al-rich inclusions in carbonaceous chondrites: Proc. 8th Lunar Sci. Conf., p. 95–112.

———, and ——— 1982, The nature and origin of type B1 and B2 Ca-Al-rich inclusions in the Allende meteorite: Geochim. Cosmochim. Acta, v. 46, p. 2581–2594.

WASSERBURG, G. J., and PAPANASTASSIOU, D. A., 1982, Some short-lived nuclides in the early solar system—a connection with the placental ISM, *in* BARNES, C. A.; CLAYTON, D. D.; and SCHRAMM, D. N., eds., Essays in Nuclear Astrophysics: London, Cambridge University Press, p. 77–140.

WEILL, D. F.; STEBBINS, J. F.; HON, R.; and CARMICHAEL, I. S. E., 1980, The enthalpy of fusion of anorthite: Contrib. Mineral. Petrol., v. 74, p. 95–102.

WOOD, J. A., 1983, Formation of chondrules and CAI's from interstellar grains accreting to the solar nebula, *in* Proc. 8th Symp. Antarctic Meteorites: Mem. Natl. Inst. Polar Res., Tokyo, in press.